



# Impact of Propellant Species on Hall Effect Thruster Electrical Facility Effects

Jason D. Frieman,<sup>\*</sup> Nathan P. Brown,<sup>†</sup> Connie Y. Liu,<sup>‡</sup> Thomas M. Liu,<sup>§</sup> and Mitchell L. R. Walker<sup>¶</sup>

*Georgia Institute of Technology, Atlanta, Georgia 30332*

Vadim Khayms<sup>\*\*</sup>

*Lockheed Martin Space Systems Company, Sunnyvale, California 94089*

and

David Q. King<sup>††</sup>

*Aerojet Rocketdyne, Inc., Redmond, Washington 98052*

DOI: 10.2514/1.B36566

**The impact of propellant species on the role of the conductive vacuum chamber wall in the discharge circuit of the 200 W T-40 Hall effect thruster is experimentally investigated using xenon and krypton propellants at operating pressures of  $1 \times 10^{-6}$  torr. Aluminum plates are placed adjacent to, but electrically isolated from, the facility walls downstream along thruster centerline and radially outward, centered on the exit plane. Data are acquired for four plate electrical configurations: 1) biased relative to ground with measurements of collected current, 2) grounded with measurements of currents to ground, 3) floating with measurements of floating voltages, and 4) connected with measurements of the current conducted between the plates. The 42% decrease in ion beam current associated with krypton operation resulted in a 58 and 19% decrease in the collected current to ground and floating voltage, respectively, of the axial plate; the 10% increase in divergence half-angle with krypton propellant yielded a change in sign for the collected current to ground and floating voltage of the radial plate. These findings suggest that changes to the ion current density profile cause concomitant changes to electrical coupling between the Hall effect thruster and test facility.**

## Nomenclature

$G$	=	gas correction factor
$I$	=	current, A
$I_p$	=	current collected by plate, A
$P_b$	=	vacuum chamber base pressure, Torr
$P_c$	=	corrected vacuum chamber background pressure, Torr
$P_i$	=	indicated vacuum chamber background pressure, Torr
$V$	=	voltage, V
$V_{cg}$	=	cathode-to-ground voltage, V
$V_p$	=	plasma potential with respect to ground, V
$\rho$	=	Pearson correlation coefficient
$\sigma_i$	=	standard deviation of waveform $i$

## I. Introduction

**T**HE high specific impulse, thrust efficiency, and thrust density provided by Hall effect thrusters (HETs) make them an appealing choice for use as the primary propulsion system on board a number of commercial and government Earth-orbiting satellite missions. In addition to the mass savings offered by these performance attributes, developments in in-space power and the growing western flight heritage portfolio of HETs have also increasingly made them prime candidates for more ambitious deep space missions [1].

The growth in interest and popularity of HETs has caused a corresponding increase in HET research, testing, and development programs both domestically and internationally [2–4]. Despite the similarities among the devices tested and measurements recorded at each of these facilities, the wide range of facility geometries, sizes, materials, and pumping capacities makes it difficult for researchers to compare datasets without the inclusion of facility-dependent corrections [5–23]. It is therefore desirable to develop an understanding of how to quantify facility effects on HET operation and data collection so that facility-dependent testing artifacts can be corrected for and a facility-independent understanding of the device performance can be achieved.

Although several investigations into facility effects exist in the literature, most focus on the role of facility backpressure on plume properties and device operation. Previous studies have shown that increases in facility pressure result in artificial increases in device thrust and efficiency due to neutral ingestion or entrainment [5–14,16,17,20–22]. Work has also been conducted linking background pressure to parasitic facility effects caused by resonant charge exchange (CEX) collisions. Specifically, studies have shown that higher facility pressures lead to increased CEX collisions; these CEX interactions introduce additional plume components and artificially increase the ion current density measured by Faraday probes in the regions of the HET plume at large angles with respect to the centerline [7,15,18,19]. These observations prompted several proposals concerning how to correct these ion current density measurements for the facility background pressure [6,8,11,15,16,19,24]. This body of experimental evidence on facility backpressure effects motivates the need to develop a process by which to calibrate any vacuum facility in terms of pressure [25].

HET test facility walls are also almost ubiquitously metallic and, as such, have finite electrical conductivity. Recent work has indicated

Received 1 December 2016; revision received 14 August 2017; accepted for publication 3 September 2017; published online 16 November 2017. Copyright © 2017 by Jason David Frieman. Published by the American Institute of Aeronautics and Astronautics, Inc., with permission. All requests for copying and permission to reprint should be submitted to CCC at [www.copyright.com](http://www.copyright.com); employ the ISSN 0748-4658 (print) or 1533-3876 (online) to initiate your request. See also AIAA Rights and Permissions [www.aiaa.org/randp](http://www.aiaa.org/randp).

<sup>\*</sup>Graduate Research Assistant, Aerospace Engineering, High-Power Electric Propulsion Laboratory, 270 Ferst Drive; [jfrieman3@gatech.edu](mailto:jfrieman3@gatech.edu). Student Member AIAA.

<sup>†</sup>Graduate Research Assistant, Aerospace Engineering, High-Power Electric Propulsion Laboratory, 270 Ferst Drive; [nbrown44@gatech.edu](mailto:nbrown44@gatech.edu). Student Member AIAA.

<sup>‡</sup>Graduate Research Assistant, Aerospace Engineering, High-Power Electric Propulsion Laboratory, 270 Ferst Drive; [cylu@gatech.edu](mailto:cylu@gatech.edu). Student Member AIAA.

<sup>§</sup>Research Engineer II, Aerospace Engineering, High-Power Electric Propulsion Laboratory, 270 Ferst Drive; [thomas.liu@ae.gatech.edu](mailto:thomas.liu@ae.gatech.edu). Member AIAA.

<sup>¶</sup>Professor, Aerospace Engineering, High-Power Electric Propulsion Laboratory, 270 Ferst Drive; [mitchell.walker@ae.gatech.edu](mailto:mitchell.walker@ae.gatech.edu). Associate Fellow AIAA.

<sup>\*\*</sup>Electric Propulsion Architect, 1111 Lockheed Martin Way; [vadim.khayms@lmco.com](mailto:vadim.khayms@lmco.com). Member AIAA.

<sup>††</sup>Technical Fellow, Engineering; currently Principal Propulsion Engineer, Space Exploration Technologies Corporation, 18390 NE 68th St., Redmond, WA 98052; [davidqking@gmail.com](mailto:davidqking@gmail.com). Member AIAA.

that the electrical conductivity of the chamber plays a significant role in the HET electrical circuit, and consequently represents an electrical facility effect [23,26–29]. Specifically, this work has shown that the facility walls collect a significant fraction of the discharge current, thereby acting as an alternate recombination site for plume ions and electrons that have not undergone recombination before reaching the facility walls. Although the current collection by the facility walls is controlled by the wall sheath and does not impact quasi-neutrality in the plume, this alternate electron recombination pathway is an artificial effect introduced by the presence of the vacuum facility that is expected to be absent on orbit. Furthermore, previous work has confirmed that the presence of this alternate pathway can alter processes dependent on the electron path through the plasma, such as cathode coupling and plasma reactance, [26–29].

The majority of the archival work on facility effects (both electrical and pressure) has been conducted using HETs operating with xenon propellant [26–29]. Although xenon is the most common choice for HET propellant, the scarce quantity and increasing demand for xenon has sparked interest in other potential HET propellant options. One of these alternatives is krypton (Kr). As compared to xenon (Xe), krypton is more abundant in the atmosphere, and thus is less expensive to obtain than xenon [30]. In addition, the atomic mass of krypton is 83.8 atomic mass units (amu), which is smaller than the 131.3 amu atomic mass of xenon. Krypton thus has increased mobility and longer mean free paths relative to xenon [31]. These properties have been shown to change the sensitivity of krypton-operated HETs to backpressure effects [32]. Because the electrical coupling between the HET and the facility is enabled by the fact that the recombination mean free path is longer than the chamber dimensions, it is expected that use of krypton and its longer mean free paths relative to xenon will similarly alter the sensitivity of the HET to electrical facility effects. However, as of yet, no work has been done to examine how propellant selection alters the HET-facility electrical coupling.

This work experimentally characterizes and compares the electrical coupling between the krypton-operated T-40 HET and the conductive walls of the vacuum test facility. A representative facility testbed with controllable wall bias is created by placing two large square aluminum plates adjacent to, but electrically isolated from, the walls of the vacuum test facility, both axially downstream and radially outward from the exit plane of the 200 W Aerojet Rocketdyne T-40 HET. Identical measurements (i.e., the current conducted through the plates and the voltage to which the plates are biased as the plates are electrically isolated, connected, and grounded) are taken for the T-40 operating on xenon and krypton in order to determine how the coupling between the HET and facility changes as a function of propellant species.

## II. Experimental Setup

### A. Vacuum Facility

All experiments were performed in Vacuum Test Facility 2 (VTF-2) at the Georgia Institute of Technology High-Power Electric Propulsion Laboratory. A schematic of this facility is shown in Fig. 1. VTF-2 is a stainless-steel chamber measuring 9.2 m in length and 4.9 m in diameter. VTF-2 is evacuated to a rough vacuum using one 495 ft<sup>3</sup>/min rotary-vane pump and one 3800 ft<sup>3</sup>/min blower. High vacuum is achieved using 10 CVI TM (Torr Master) reentrant cryopumps. The cryopump shrouds are fed using the Stirling Cryogenics SPC-8 RL special closed-loop nitrogen liquefaction system detailed by Kieckhafer and Walker [33]. The facility has a combined nominal pumping speed of 350,000 l/s on xenon and can achieve a base pressure of  $1.9 \times 10^{-9}$  torr. The pressure in VTF-2 was monitored using two Agilent Bayard-Alpert (BA) 571 hot-filament ionization gauges controlled by an AgilentXGS-600 gauge controller. One gauge was mounted to a flange on the exterior of the chamber, whereas the other was mounted 0.6 m radially outward and centered 0.3 m upstream of the HET exit plane. To prevent plume ions from having a direct line of sight to the ionization gauge filament of the interior ion gauge and potentially affecting the pressure measurement, a neutralizer identical to the one used by Walker and Gallimore was

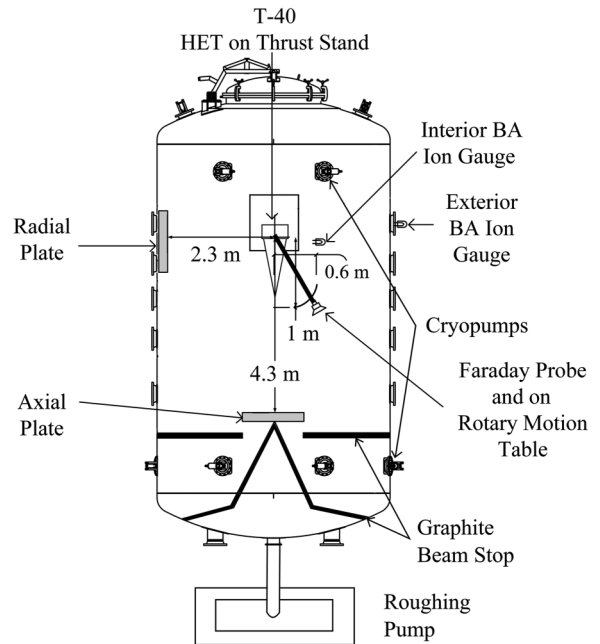


Fig. 1 Schematic of VTF-2 (not to scale).

attached to the gauge orifice [25]. The nominal operating pressure for this work as measured by the interior ion gauge was  $8.9 \times 10^{-7}$  torr and  $1.1 \times 10^{-6}$  torr for krypton and xenon operation, respectively; for the exterior ion gauge, the nominal operating pressure was  $1.0 \times 10^{-6}$  torr and  $1.2 \times 10^{-6}$  torr, respectively. It is important to note that these operational pressures are among the lowest published for any HET facility effects evaluation [5–14,16,17,20–22,34]. All reported pressures are corrected for the employed propellant; the corrected pressure  $P_c$  is found by relating the indicated pressure  $P_i$  and the vacuum chamber base pressure  $P_b$  to a gas-specific correction factor  $G$  using the following equation:

$$P_c = \left[ \frac{P_i - P_b}{G} \right] + P_b \quad (1)$$

where  $G$  is equal to 2.87 for xenon and 1.96 for krypton [35].

### B. T-40 HET

All experiments detailed in this work were performed using the Aerojet Rocketdyne T-40 HET originally developed by Space Power, Inc., in collaboration with the Keldysh Research Center and Matra Marconi Space [36]. The T-40 HET is a laboratory-model HET with a design operational power range of 50–300 W [34,36]. To address the loss mechanisms relevant for low-power HET operation, the T-40 HET leverages design heritage from the Aerojet Rocketdyne 3.4 kW T-140 HET as well as a patented magnetic circuit design [36]. The performance of the T-40 HET operating with krypton and xenon has been mapped by prior investigations [34]. To be consistent with previous work with xenon propellant, the thruster body was electrically grounded to the vacuum chamber.

High-purity (99.9995%) xenon and krypton propellants were supplied to the thruster and cathode using stainless-steel lines metered with MKS 1179A mass flow controllers. The controllers were calibrated before each test by measuring gas pressure and temperature as a function of time in a known control volume. The mass flow controllers have an uncertainty of  $\pm 0.01$  mg/s for both the cathode and anode flows [36].

To be consistent with past work with the T-40 HET, a 10 A Moscow Aviation Institute (MAI)-derived lanthanum hexaboride (LaB<sub>6</sub>) cathode was used for this work [34,37]. The MAI cathode was located at the 12 o'clock position of the thruster. The cathode volumetric flow rate was constant for all thruster operating conditions. The orifice location of the cathode was located approximately 2.2 cm downstream

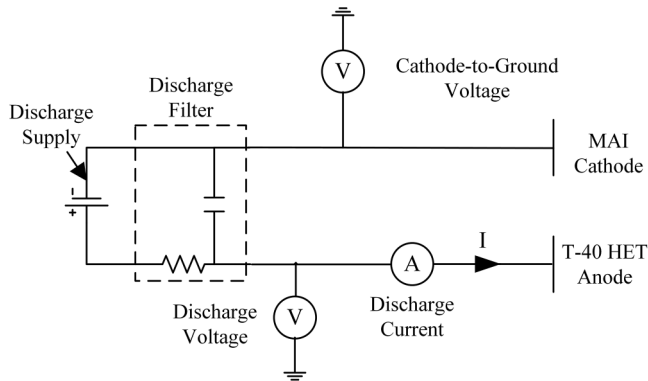


**Fig. 2** T-40 HET circuit and thruster telemetry measurement locations.

of the thruster exit plane and 4.1 cm radially outward from the thruster centerline. The cathode was set at a fixed declination of 45 deg with respect to the thruster centerline. It is important to note that the employed MAI cathode was approximately three times larger in terms of maximum emission current and flow rate than the nominal T-40 HET cathode and other cathodes typically coupled to low-power HETs. The impacts of this on HET operation were discussed in previous work [34].

The magnetic circuit configuration of the T-40 HET, which is composed of two concentric coils centered on the thruster centerline, restricts the position of the magnetic field separatrix to the thruster centerline and precludes the T-40 HET from exhibiting the off-centerline separatrix surfaces shown in HETs with magnetic coils centered off-axis [27,38]. The T-40 magnetic field topology thus eliminates any concerns about near-field plume properties and cathode coupling as a function of cathode position relative to off-centerline separatrix surfaces [39].

The T-40 HET discharge was controlled using a Magna-Power TSA800-54 power supply; the inner and outer magnets were powered using TDK-Lambda GEN60-25 power supplies. A TDK-Lambda GEN600-2.6 and GEN40-38 were used for the cathode keeper and heater, respectively. All electrical connections entered VTF-2 through separate feedthroughs to eliminate potential electromagnetic interference concerns. The thruster discharge supply was connected

to a discharge filter consisting of a 95  $\mu\text{F}$  capacitor and 1.3  $\Omega$  resistor to prevent oscillations over 1.4 kHz in the discharge current from reaching the discharge supply. Figure 2 shows the circuit used for the T-40 HET in this work.

The mean discharge voltage and cathode-to-ground voltage of the T-40 HET were measured differentially using a pair of Teledyne LeCroy PPE2 kV 100:1 high-voltage probes connected to a Teledyne LeCroy HDO6104 oscilloscope with an uncertainty and bandwidth of  $\pm 0.5\%$  full scale and 1 GHz, respectively. The discharge current oscillations of the T-40 HET were recorded using a Teledyne LeCroy CP030 current probe connected to the same Teledyne LeCroy oscilloscope. The minimum sensitivity, maximum noise, and bandwidth of the current probe were 10 mA/division, 2.5 mA<sub>rms</sub>, and 50 MHz, respectively. To minimize the uncertainty associated with shifts in the zero reading, the employed CP030 current probe was degaussed before acquisition of all data and at approximately 30 min intervals during HET operation. To verify the employed measurement technique, the current probe and oscilloscope were calibrated using a Keithley 2410 1100 V SourceMeter with an accuracy of  $\pm 1 \mu\text{A}$ . These calibrations indicated a combined average uncertainty of approximately 15% for currents below 20 mA and 7.5% for currents between 20 mA and 0.1 A. Figure 2 shows the location of each telemetry measurement in the T-40 HET circuit.

### C. Configuration of Plates

To simulate a metallic facility with controllable wall bias, two 0.91 m  $\times$  0.91 m  $\times$  0.16-cm-thick square aluminum plates were mounted adjacent to, but electrically isolated from, the walls of the vacuum test facility. The axial plate was located 4.3 m downstream from the exit plane of the thruster. The radial plate was located 2.3 m radially outward from the thruster centerline and was centered on the exit plane of the T-40 HET. Figure 1 shows the physical location of the plates with respect to the T-40 HET. Identical plates have been used in previous studies of electrical facility effects [26–29]. The surface area of the plates represents approximately 2% of the total facility wall area.

Figure 3 shows each of the four plate electrical configurations used in this test. In all four cases, the electrical connection to the plate is made using a RG-58 coaxial cable with a grounded shield. This transmission line is similar to those that have been used previously

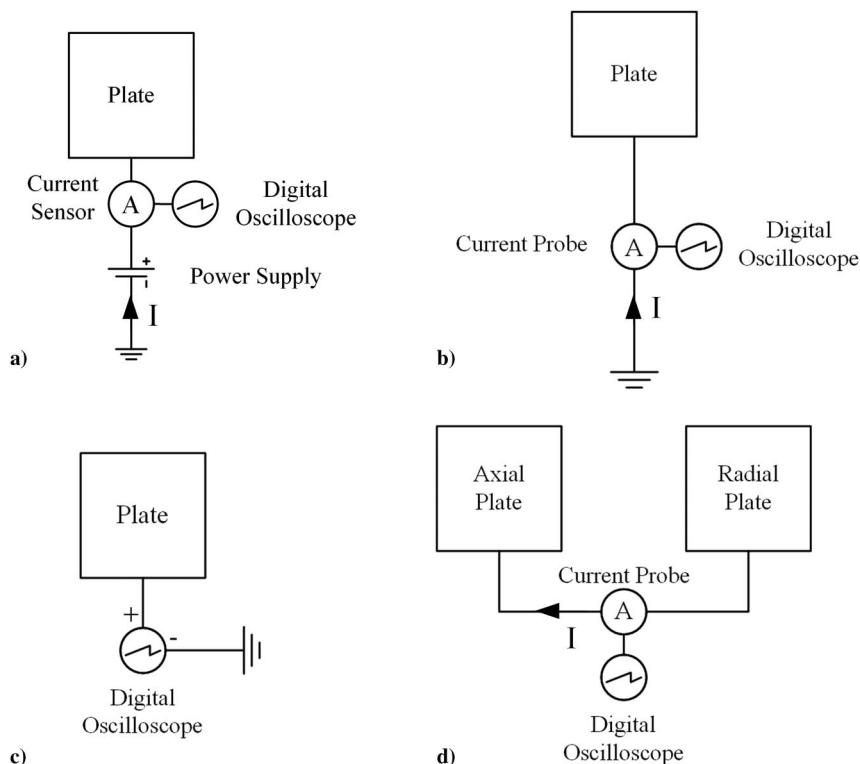


**Fig. 3** Plate circuit configurations: a) I-V swept, b) grounded, c) floating, and d) connected.

to study HET discharge oscillations [40,41]. In configuration A [current–voltage (I–V) swept], each plate was effectively used as a large planar Langmuir probe [42,43]. The bias voltage was controlled using a TDK-Lambda GEN150-10 power supply, and the plate current was measured using a Teledyne LeCroy CP030 current sensor connected to the Teledyne LeCroy HDO6104 oscilloscope. In configuration B (grounded), each plate was directly connected to the chamber ground with the current conducted between each plate and ground measured with a Teledyne LeCroy CP030 current sensor connected to the Teledyne LeCroy HDO6104 oscilloscope. In configuration C (floating), the plates were electrically isolated, and the floating voltage was measured directly using a Teledyne LeCroy PP018 passive probe connected to the Teledyne LeCroy oscilloscope. Consistent with previous work, in configurations A, B, and C, the plate not actively being biased was electrically floating. In configuration D (connected), the plates were connected to each other instead of to the ground, and the current conducted between the two plates was measured with a Teledyne LeCroy CP030 current probe connected to the Teledyne LeCroy oscilloscope. For all plate configurations, the electrical measurements and thruster telemetry signals were measured simultaneously at a sampling frequency of 2.5 GS/s for 500  $\mu$ s to eliminate any potential phasing effects that could result from asynchronous sampling.

#### D. Faraday Probe

The ion current density profile was measured using a Faraday probe [7,15]. The ion beam current and plume divergence half-angle were calculated through analysis of the measured ion current density profiles. The Faraday probe consisted of a pair of electrostatically biased electrodes that measured the spatially resolved ion current density as the probe was traversed along a constant-radius arc. These current density measurements were spherically integrated to determine the ion beam current and plume divergence half-angle. For this work, the Faraday probe was placed on an arc located 1 m downstream of the exit plane of the HET and swept from  $-90$  to  $90$  deg relative to the thruster centerline at a speed of 2 deg/s. The distance between measurements was approximately 0.5 deg. The location of the Faraday probe along the arc was controlled using a Parker Daedel 200RT series rotary table, which has a positional uncertainty of  $\pm 0.17$  deg.

A Jet Propulsion Laboratory-style nude Faraday probe similar in design to the one previously used by Walker et al. [19] and Xu [44] was used for this work. The probe consisted of a tungsten-coated aluminum collector that was 2.31 cm in diameter, surrounded by an aluminum shield electrode with a 1.15 mm gap distance. Consistent with previous investigations of the T-40 HET, the guard and collector were both biased to  $-30$  V using a Xantrex XEL 60-1.5 power supply. The collector signal was passed through a 100  $\Omega$  shunt, and the resultant voltage drop across the resistor was measured using an Agilent 34970A data acquisition/data logger switch unit (hereafter referred to as (DAQ) to determine the current collected by the Faraday probe. The angular traverse of the probe through the plume and the DAQ were simultaneously controlled using a LabVIEW virtual instrument to ensure synchronous recording of the angular position of the probe and the spatially resolved collected current.

To reduce any systematic directional bias, two angular sweeps of the Faraday probe were taken in succession at each measurement condition in opposing directions (i.e., one sweep was taken each from  $-90$  to  $90$  deg and from  $90$  to  $-90$  deg). The recorded data were analyzed using the correction factors and methods detailed by Brown and Gallimore [7]. The reported ion beam currents and plume divergence half-angles represented the average of the results computed for each of the two angular sweeps taken for every thruster/plate configuration. The uncertainty associated with this method was approximately 5% for the beam current and 1.5% for the plume divergence half-angle [7,15].

### III. Results and Discussion: HET–Plate Coupling

This section examines the impact of propellant species on the electrical interaction between the T-40 HET and the conductive walls of the test facility by presenting data collected during krypton

operation and comparing them to analogous data collected during xenon operation. All data were collected with the thruster operating at a constant anode volumetric flow rate of 11.7 standard cubic centimeters per minute (scm) (equivalent to 1.14 mg/s xenon or 0.73 mg/s krypton), a cathode volumetric flow rate of 9.3 scm (equivalent to 0.91 mg/s xenon or 0.58 mg/s krypton), and a discharge voltage of 250 V, yielding discharge powers of 225 and 168 W for xenon and krypton operation, respectively. In this work, the HET discharge voltage, inner and outer magnet currents, anode volumetric flow rate, and cathode volumetric flow rate were held constant for all plate configurations. To minimize uncertainty, data were collected without breaking vacuum between operation with the two propellants. It should be noted that the plate current sign convention was chosen such that a net electron current was positive in order to maintain consistency with the sign convention typically used to describe Langmuir probe I–V characteristics [27,42]. This is the same sign convention employed in Fig. 3.

Before presenting the results, a discussion is warranted regarding the implications of operating the T-40 HET with matched xenon and krypton volumetric flow rates. Although there have been several investigations into HET operation with krypton, overall, there is no consensus regarding the most appropriate parameter to match to compare xenon and krypton operations [45–47]. Matching volumetric flow rates results in the injection of the same number of neutral particles during both xenon and krypton operations, thereby yielding equivalent near-field pressures for similar neutral temperatures [45]. This pressure equivalency is important because previous work indicated that electrical facility effects may be sensitive to the neutral pressure distribution in the facility [28,48]. The choice to match either mass flow rates or discharge powers (which are the two other common methods for krypton operation) was avoided because it would have yielded an increase in number density of 25–60%, and therefore could have resulted in the conflation of electrical and backpressure effects and altered the relative current collected by the axial and radial plates [28,45,48]. Furthermore, the published T-40 HET throttle table for krypton is populated using matched volumetric flow rates, thus providing a known baseline for comparison [34].

#### A. Ion Current Density Profiles

Because the focus of this work is the electrical coupling between the conductive facility walls and the HET plume, it is useful to examine how the plume ion current density profile changes between operation with xenon and krypton before presenting the data collected using the test plates [29]. The ion current density profiles of the T-40 HET for operation with xenon and krypton are shown in Fig. 4 as a function of the Faraday probe position. The centerline ion current density, divergence half-angle, and ion beam current of the T-40 HET are approximately 1.9 A/m<sup>2</sup>, 30 deg, and 0.76 A,

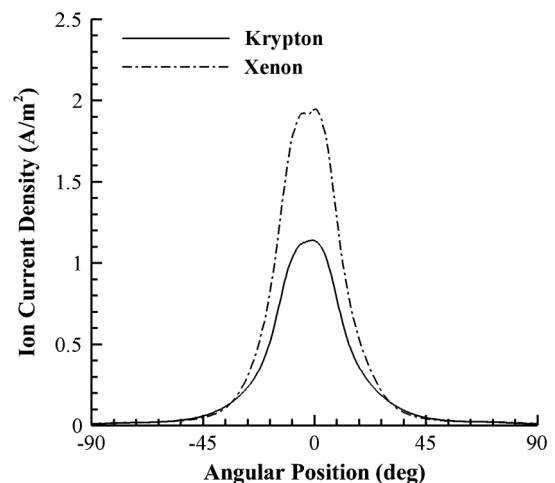


Fig. 4 Representative T-40 HET ion current density profiles.

respectively, for xenon operation and  $1.1 \text{ A/m}^2$ ,  $33 \text{ deg}$ , and  $0.57 \text{ A}$ , respectively, for krypton operation. The T-40 HET is optimized for the current densities associated with the xenon operation; therefore, the higher divergence half-angle, along with lower beam current and centerline ion current density during krypton operation, are consistent with the findings of previous studies [34,45].

These results can be used to compute the current utilization efficiency of the T-40 HET. The current utilization efficiency is defined as the ratio of the ion beam current to the discharge current and is a measure of how efficiently the electrons are used to ionize the propellant [49]. For operation with both xenon and krypton, the current utilization efficiency of the T-40 HET is approximately  $84 \pm 5\%$ . This observed invariance in current utilization efficiency between xenon and krypton operation is consistent with previous work and indicates that (within the uncertainty of the measurements) the percentage of the discharge current composed of beam ions is the same between krypton and xenon operations [50].

### B. Grounded Plate Configuration

The impact of the aforementioned changes in the plume ion current density profile on the electrical coupling between the HET and test facility as a function of propellant species can be quantified by analyzing the data acquired with the test plates in each of the configurations shown in Fig. 3. The discharge current and current collected by the grounded axial and radial plates for the xenon-operated T-40 HET are shown in Figs. 5a and 5b, respectively; the same data are shown for the krypton-operated T-40 HET in Figs. 5c and 5d, respectively. During xenon operation,  $-0.050 \text{ A}$  (5.7% of the discharge current) was collected by the grounded axial

plate and  $0.001 \text{ A}$  ( $-0.13\%$  of the discharge current) of current was collected by the grounded radial plate. During krypton operation, the grounded axial plate collected an average current of  $-0.021 \text{ A}$  (3% of the discharge current) and the grounded radial plate collected an average current of  $-0.007 \text{ A}$  (0.9% of the discharge current). Although the axial plate collected net ion current for both propellants, the radial plate collected a net electron current during xenon operation and a net ion current during krypton operation. For both propellants, the magnitude of the current collected by the axial plate was greater than that collected by the radial plate.

The fact that the magnitude of the current collected by the grounded axial plate was higher than that collected by the grounded radial plate for both propellants can be explained by the spatial configuration of the plates [26,27]. The axial plate is located downstream of the centerline of the HET and, as shown in Fig. 4, is therefore directly impinged upon by the densest region of HET plume ions [51]. The radial plate, on the other hand, is located in the angular wings of the HET plume, and subsequently receives less direct impingement from plume ions; this results in the radial plate collecting a smaller magnitude current [7,15,18,19].

The change in radial plate current collection from net electron current for xenon operation to net ion current for krypton operation can be explained by the concomitant change in the plume divergence half-angle associated with the change in propellant. As discussed in Sec. III.A and in previous work with HETs operating with krypton propellant, the plume divergence half-angle is larger during krypton operation than xenon operation for matched volumetric flow rates and discharge voltages [34,45]. Thus, a smaller percentage of primary ions are accelerated off-axis during xenon operation and the plasma near the

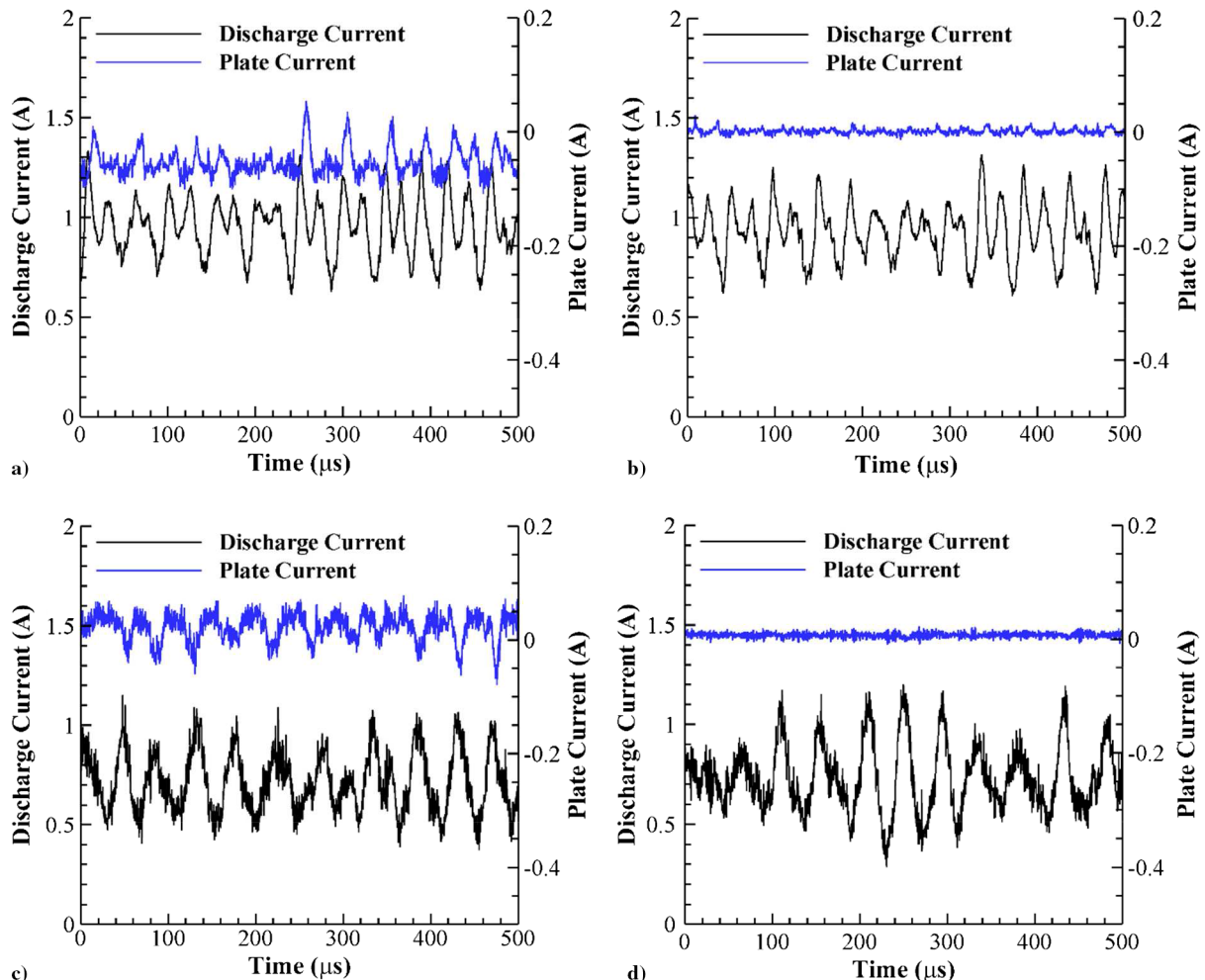
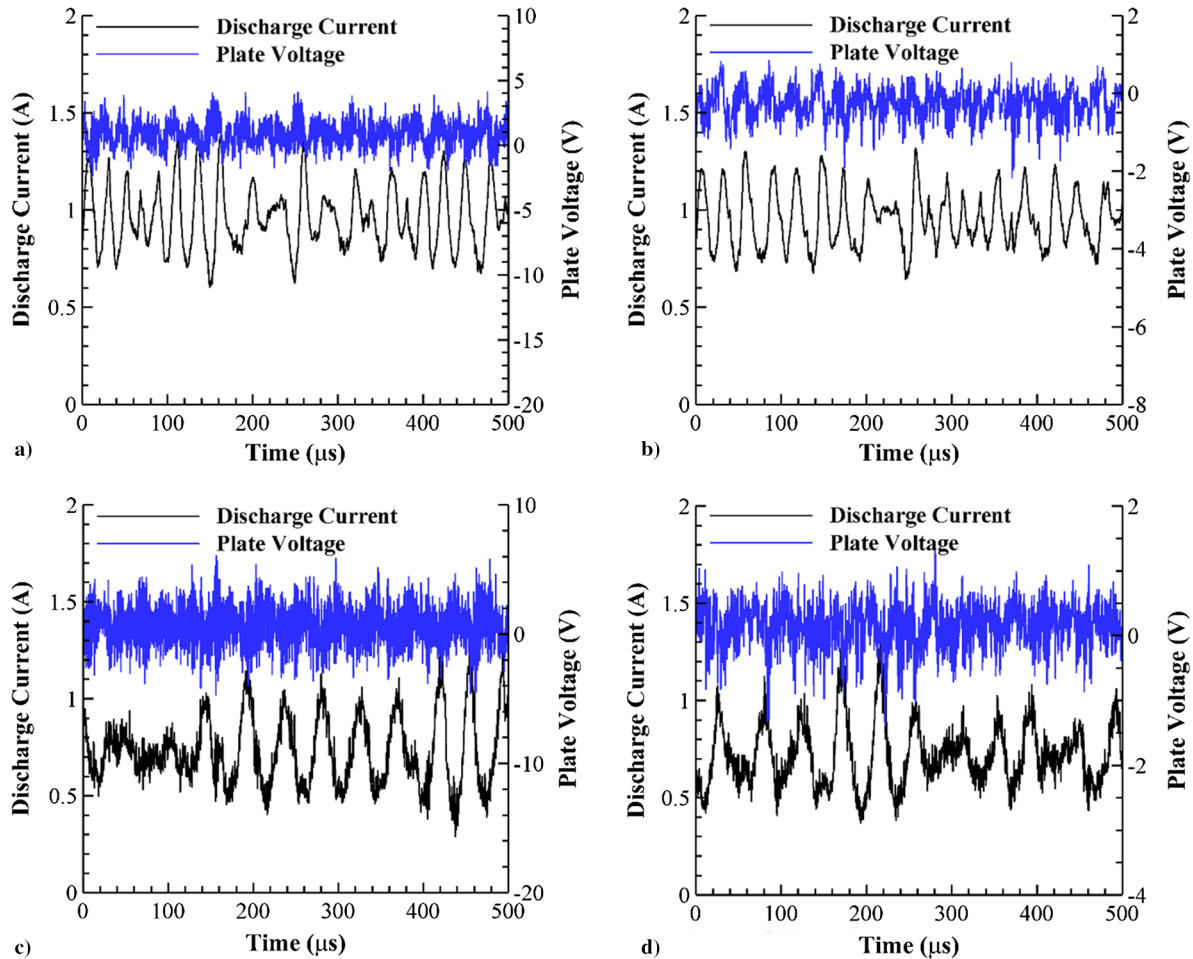


Fig. 5 Discharge and current collected by the grounded a) axial and b) radial plates for xenon operation and c) axial and d) radial plates for krypton operation.



**Fig. 6** Discharge current and plate floating voltage for the a) axial and b) radial plates for xenon operation and the c) axial and d) radial plates for krypton operation.

radial plate is composed primarily of CEX ions and electrons. Because the electrons are the more mobile species, a net electron current is collected by the grounded radial plate [28]. The increase in divergence half-angle indicates that a larger percentage of ions is accelerated off-axis for krypton operation. This increase in off-axis acceleration sufficiently increases the effective ion mobility toward the radial plate and results in the grounded radial plate collecting a net ion current.

As shown in Fig. 5, the grounded axial plate collected more than twice as much current during xenon operation as compared to krypton operation. This result is expected because the discharge current of the xenon-operated T-40 HET is larger for operation at matched volumetric flow rates due to the reduced ionization cost and larger ionization cross sections of xenon relative to krypton [30]. A more meaningful comparison is therefore between the percentages of the discharge current collected by each plate for each propellant species. The grounded axial plate collected a larger percentage of the discharge current for xenon operation. The reason for this is related to the results from the floating plate configuration and is discussed in Sec. III.C. By contrast, the grounded radial plate collected a larger percentage of the discharge current for krypton operation. This result is consistent with the increase in off-axis ion acceleration associated with krypton operation (i.e., operation with krypton produces a larger beam divergence half-angle, and consequently results in an increase in effective mobility toward the radial plate). It is important to note that implicit in the preceding discussion is the assumption that the observed changes in normalized current collection are driven by changes in the ion beam current and not in the percentage of the discharge current composed of beam ions. Because the current utilization efficiency did not change between operation with krypton and xenon (as discussed in Sec. III.A), it is expected that the error associated with this assumption is minimal.

### C. Floating and Connected Plate Configurations

Figures 6a and 6b show the discharge current and axial and radial plate floating voltages, respectively, for the T-40 HET operating with xenon propellant; and Figs. 6c and 6d show these data for operation with krypton propellant. For xenon operation, the floating voltages were 0.85 and  $-0.29$  V for the axial and radial plates, respectively; for krypton operation, the floating voltage of the axial plate was 0.69 V and the floating voltage of the radial plate was 0.13 V. The magnitude of the axial plate floating voltage was higher than the radial plate floating voltage for both propellants due to the spatial configuration of the plates, as discussed previously.

Although the signs are the same, the magnitude of the axial plate floating voltage is greater during operation with xenon than with krypton. Thus, in the grounded configuration, the axial plate bias is closer to the floating voltage during krypton operation. The ion current density profiles of the thruster plumes, shown in Fig. 4, provide an explanation for the larger axial plate floating voltage observed during xenon operation. As noted in Sec. III.A, the centerline ion current density of the T-40 HET is approximately  $1.9$  A/m<sup>2</sup> for xenon operation and  $1.1$  A/m<sup>2</sup> for krypton operation. The larger ion current density observed during xenon operation results in the direct impingement of a larger number of ions on the axial plate, and thereby necessitates that the axial plate float to a higher floating voltage in order to maintain net zero current collection [43]. This suggests that changes in centerline ion current density drive the observed changes in electrical coupling between the HET plume and the axial plate.

As noted previously, the radial plate floating voltage is positive for krypton operation and negative for xenon operation. These results are consistent with those presented for the grounded plate configuration in which a net ion current was collected for krypton operation,

whereas a net electron current was collected for xenon operation. The difference in signs between the floating voltages measured for each propellant is driven by the differences in plume divergence. Operation with krypton produces a larger beam divergence half-angle. As previously discussed, this results in an increase in effective ion mobility toward the radial plate and requires that the plate float to a positive voltage to maintain the net zero current condition. As the beam divergence half-angle is a characteristic of the shape of the ion current density profile, these results suggest that the shape of the ion current density profile, and not simply the centerline ion current density, must be accounted for in order to understand the electrical coupling of the HET plume with the radial facility surfaces.

Further evidence of the influence of plume shape and centerline current density on the electrical coupling between the HET and facility is provided by the results of the connected plate configuration. Figures 7a and 7b show the net current flowing between the connected plates for the xenon- and krypton-operated T-40 HETs, respectively. The current flowing between the connected plates was 0.016 A (1.7% of the discharge current) during xenon operation and 0.005 A (0.7% of the discharge current) during krypton operation. Because the potential difference between the axial and radial plates was larger during xenon operation, and this voltage difference was what drove the current conducted between the connected plates, the corresponding plate-to-plate current was also larger.

#### D. I-V Swept Plate Configuration

To further characterize the impact of propellant selection on the coupling between the HET and facility, I-V sweeps were taken to show how the current collected by the plates varies as a function of plate bias

voltage. These results are shown in Figs. 8a and 8b, which display the current collected by the axial and radial plates, respectively, as a function of plate bias during T-40 HET operation with krypton and xenon. During operation with both propellants, the I-V characteristics of the axial and radial plates demonstrate the three regions typical of planar Langmuir probe characteristics (i.e., ion saturation, transition, and electron saturation) [42,43]. It is important to note that the grounded and floating plate results detailed previously can be recovered from the I-V characteristics and that the two datasets are therefore consistent.

As shown in Figs. 8a and 8b, the ion saturation current for the axial and radial plates was  $-0.053$  and  $-0.001$  A, respectively, for krypton operation and  $-0.077$  and  $-0.002$  A, respectively, for xenon operation. As done in previous sections, these values are normalized by the discharge current, and the results are shown in Figs. 9a and 9b. These results reveal that the ion saturation current represents 7.5 and 0.2% of the discharge current for the axial and radial plates, respectively, during krypton operation and 8.0 and 0.2% of the discharge current for the axial and radial plates, respectively, during xenon operation. Although the collected ion saturation currents for xenon operation is approximately 45 and 100% larger in magnitude than that for krypton operation for the axial and radial plates, respectively, the difference in normalized ion saturation current between krypton and xenon operation is less than or equal to 0.5% for both plates. These values are therefore equal within the uncertainty of the measurements. Furthermore, the normalized ion saturation current matches that observed with the 3.4 kW T-140 HET in previous work, despite the fact that the T-140 was tested at an order of magnitude higher pressure [27]. This result indicates that discharge

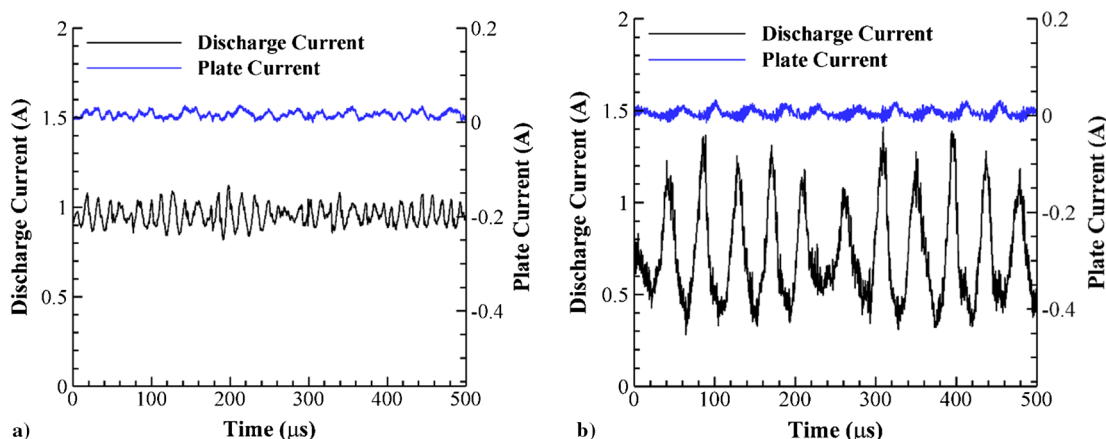


Fig. 7 Discharge current and net current flowing between the plates in the connected plate configuration for the a) xenon- and b) krypton-operated T-40 HET.

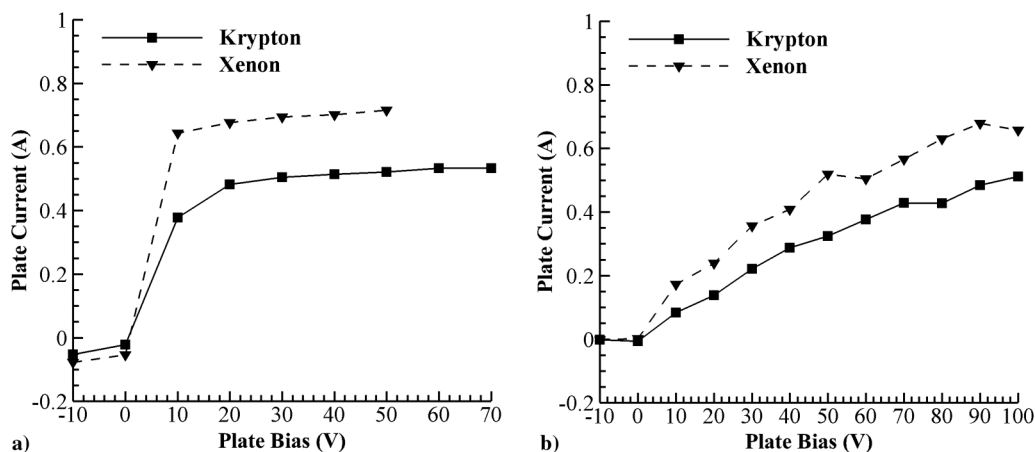
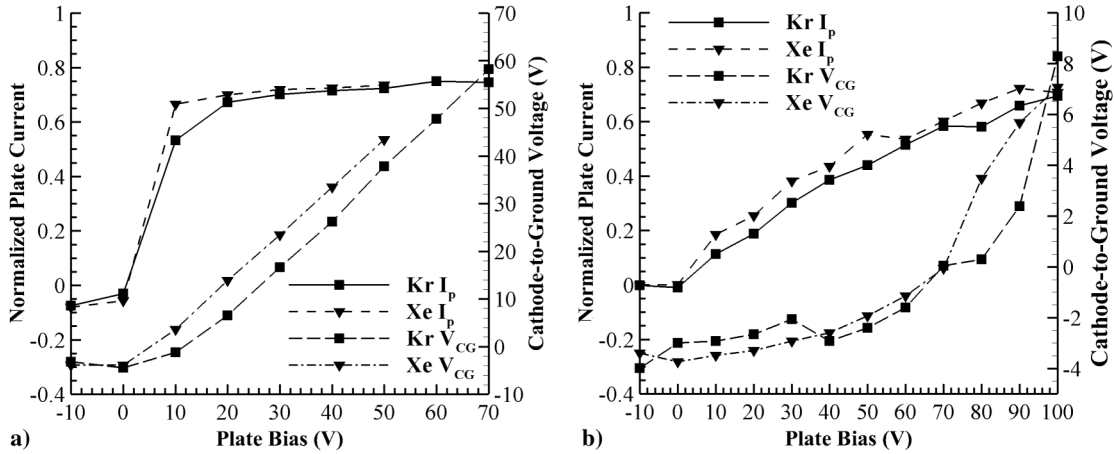


Fig. 8 Current collected by the a) axial and b) radial plates in I-V swept plate configuration.



**Fig. 9** Normalized current collected by a) axial and b) radial plates and respective T-40 HET cathode-to-ground voltage measured in the I-V swept plate configuration.

current can be used to collapse the collected ion saturation current on the test plates to a nearly universal value for this test facility.

It is important to note that these results are only strictly valid for VTF-2 at the Georgia Institute of Technology. However, insight into what may happen at other facilities can be gained by analyzing the physical processes governing current collection by these plates in the ion saturation regime. The normalized ion saturation current collected by an electrode in a plasma is proportional to the local normalized number density, ion velocity, and electrode area [43]. In this context, the term local normalized number density refers to the number density at the plate divided by the value at a reference location in the plume to correct for the changes in discharge current between the T-140 and the xenon- and krypton-operated T-40s. As discussed previously, the axial plate is directly impinged upon by the HET plume. Thus, the relevant ion velocity for ion saturation current is the mean velocity of the beam ions [27]. By estimating the beam voltage as the difference between the discharge voltage and the cathode-to-ground voltage, it can be shown that the mean beam velocity is only 5% higher for the T-140 HET in previous work as compared to the T-40 HET in this work [9]. Furthermore the ion-electron recombination mean free path for both HETs is much longer than the distance between the HET exit planes and the axial plate; thus, there should be minimal changes in the normalized number density near the plate and, for a fixed plate geometry, minimal change in the normalized ion saturation current [27,52]. Therefore, it is expected that, should similar plates be placed inside the ion-electron recombination mean free path in other facilities, a similar collapse of the normalized ion saturation current will also be observed for HETs operating at similar beam voltages.

A similar comparison of electron saturation currents can be performed for the axial plate I-V characteristics. Figure 8a shows that the axial plate electron saturation current is approximately 0.52 A during krypton operation and 0.72 A during xenon operation. When normalized by the discharge current, as shown in Fig. 9a, the electron saturation current is  $-0.73\%$  of the discharge current for krypton operation and  $-0.74\%$  of the discharge current for xenon operation. When operated with xenon, the T-40 HET produces an axial plate electron saturation current approximately 38% larger in magnitude than when operated with krypton; but, after the dependency on discharge current is removed through normalization, this difference drops to 1%.

An analysis of electron saturation current could not be performed with the radial plate I-V characteristics. Although the plate was biased to sufficiently large voltages for the I-V characteristic of both propellants to fully establish the electron saturation regime, the lack of resolution did not allow for accurate calculation of the electron saturation current [42,43]. It is important to note, however, that at a bias voltage of 100 V, the electron current collected by the radial plate was above 60% of the discharge current for both propellants, even though the radial plate was not directly impinged upon by the HET

plume. Previous work has shown that the large current collection by the radial plate at high positive bias voltages was most likely driven by sheath expansion and not changes in plume structure [29]. A detailed analysis of the impact of plate current collection on plume power was also contained in previous work [48].

**E. Cathode-to-Ground Voltage**

Previous studies have shown that, in addition to providing an alternate recombination pathway for plume ions and electrons, the biased facility walls can also impact the HET circuit potentials [26–28]. In an effort to gauge how this coupling changes as a function of propellant, Figs. 9a and 9b show the cathode-to-ground voltage of the T-40 HET as a function of test plate bias for operation with both xenon and krypton propellant. There is appreciable coupling between the plate bias voltage and the cathode-to-ground voltage during operation with both propellants. Specifically, Figs. 9a and 9b show that, at axial and radial plate biases greater than 0 V, the cathode-to-ground voltage increases monotonically with plate bias for both krypton and xenon operations. Further quantification of this relationship is provided by Fig. 10, which shows the derivative of the cathode-to-ground voltage as a function of axial plate bias for krypton and xenon operations. The derivative approaches a value of one as the axial plate bias is increased during operation with both propellants; this region of one-to-one coupling begins at a plate bias of approximately 30 V during krypton operation and 20 V during xenon operation. Previous work has shown that the onset of the one-to-one coupling region coincides with the beginning of the electron saturation regime of the I-V characteristic [53,54]. As

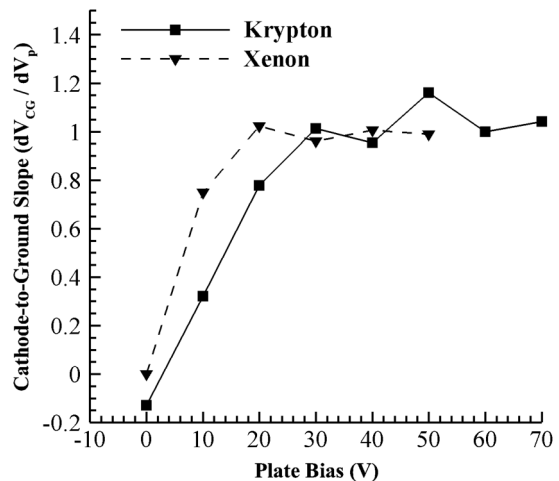


**Fig. 10** Derivative of measured T-40 HET cathode-to-ground voltage as a function of axial plate bias voltage.

shown in Fig. 8, the electron saturation regime is entered at a larger axial plate bias during krypton operation, so the later onset of the one-to-one coupling region observed during operation with krypton is consistent with previous findings.

Although coupling was also observed between the cathode-to-ground voltage and radial plate bias voltage during operation with both krypton and xenon, the cathode-to-ground voltage varied by less than 12 V (as compared to 62 V for the axial plate) across all plate biases for operation with both propellants. As noted previously and discussed in previous work, the coupling of the cathode-to-ground voltage with radial plate bias was much weaker than with axial plate bias because the radial plate received very little direct impingement from the densest portion of the HET plume. The plate could therefore collect ions at larger bias voltages before the cathode-to-ground voltage was required to increase. These results suggest that this weaker coupling was preserved even with the larger plume divergence half-angle during krypton operation. A more detailed discussion of the impact of plate bias on the plume plasma was presented in previous work [26,27].

## F. Time-Resolved Analysis

Further insight into the nature of the observed coupling between the HET and test plates can be provided by time-resolved analyses of the discharge current and collected plate current.

### 1. Discharge Current Oscillations

The stability of the HET discharge is commonly characterized by the peak-to-peak values of the discharge current [28,55]. Figures 11a and 11b show the discharge current peak-to-peak values during T-40 HET operation with krypton and xenon propellants as a function of axial and radial plate biases, respectively. The error bars shown in Figs. 11a and 11b represent the standard deviation of the measured peak-to-peak values at each individual plate bias. All time-resolved results reported in the text are listed as the mean value plus or minus one standard deviation across all plate biases.

As shown in Fig. 11a, the average peak-to-peak of the discharge current across all axial plate biases was  $0.81 \pm 0.17$  A and  $0.39 \pm 0.01$  A during krypton and xenon operations, respectively. Across all radial plate biases, as shown in Fig. 11b, the average peak-to-peak of the discharge current was  $0.68 \pm 0.12$  A for krypton operation and  $0.39 \pm 0.05$  A for xenon operation. The larger discharge current peak-to-peak values measured for the krypton-operated T-40 HET were consistent with previous results showing that, when operating with krypton, thrusters with magnetic circuit designs optimized for xenon operation (such as the T-40 HET) exhibited increased discharge current instability [45]. The peak-to-peak values of the thruster discharge current did not vary as a function of axial or radial plate bias for either krypton or xenon operation. It is important to note that an increase in discharge current peak-to-peak was observed between axial plate biases of 10 and 20 V and at a radial plate bias of 100 V. This seemingly discontinuous jump in discharge

current peak-to-peak values resembled one of the characteristics identified by Sekerak et al. to be indicative of a mode transition [56]. However, to meet the full definition of a mode transition outlined by Sekerak et al., a concomitant discontinuity would also have to be observed in the mean discharge current and peak frequency [56]. However, no such changes in either of these parameters were observed and, as such, this shift was unlikely to be due to a mode transition but, rather, may be more emblematic of the oscillatory nature of the thruster when operating with krypton. These findings therefore indicated that the stability of the T-40 HET discharge was not affected by axial or radial plate biases, regardless of whether the thruster was operated with krypton or xenon [28].

The time-resolved operating characteristics of the HET can be further quantified by the peak frequency of the discharge current [9,28,55,57]. The peak frequency is equal to the frequency of maximum power in the power spectrum that, in order to maintain consistency with previous work on HET oscillations, was obtained by applying a fast Fourier transform to the discharge current signal to decompose the time-domain signal into its components in the frequency domain [58]. The resulting peak frequencies in this work are accurate to  $\pm 2$  kHz and are plotted as a function of axial and radial plate biases, respectively, for operation with both krypton and xenon in Figs. 12a and 12b. The peak frequency of the discharge current, as shown in Fig. 12, is  $23 \pm 2$  kHz during krypton operation and  $41 \pm 3$  kHz during xenon operation across all axial and radial plate biases. The observed lower peak frequency for the krypton-operated HET is consistent with findings from previous work with thrusters of this power class [59]. Figure 12 also shows that the peak frequency of the discharge current is not dependent on plate bias for the T-40 HET when operated with either propellant.

### 2. Plate Current Oscillations

Although the time-resolved characteristics of the discharge current are unaffected by test plate bias, previous work with the T-140 HET suggests that the oscillation characteristics of the current collected by the plates are coupled to those of the discharge [26–28]. To determine whether this coupling is present for the krypton-operated T-40 HET, the peak-to-peak values and most probable frequencies of the current collected by the axial plate (shown in Figs. 13a and 13b, respectively), as a function of axial plate bias, were examined. Figure 13a shows that the average peak-to-peak values for the current collected by the axial plate are  $0.20 \pm 0.07$  A during krypton operation and  $0.19 \pm 0.06$  A during xenon operation, which are less than one-fourth and one-half, respectively, of the corresponding discharge current peak-to-peak values. Previous work has shown that fluctuations in plume properties that govern current collection, such as plasma potential and electron temperature, are dampened in the far field of the plume, so the observed decrease in peak-to-peak values is expected [60]. As shown in Fig. 13b, the average peak frequencies of the current collected by the axial plate during krypton

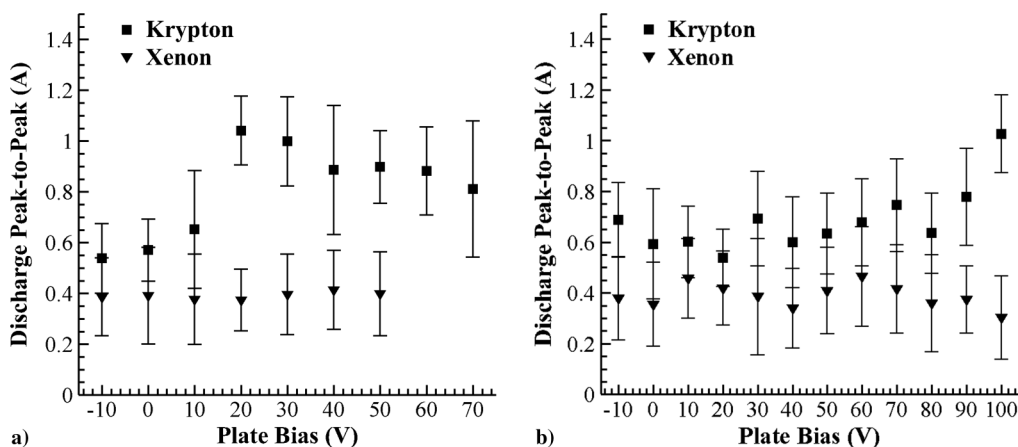


Fig. 11 Average peak-to-peak values of the T-40 HET discharge current as a function of a) axial and b) radial plate bias voltages.

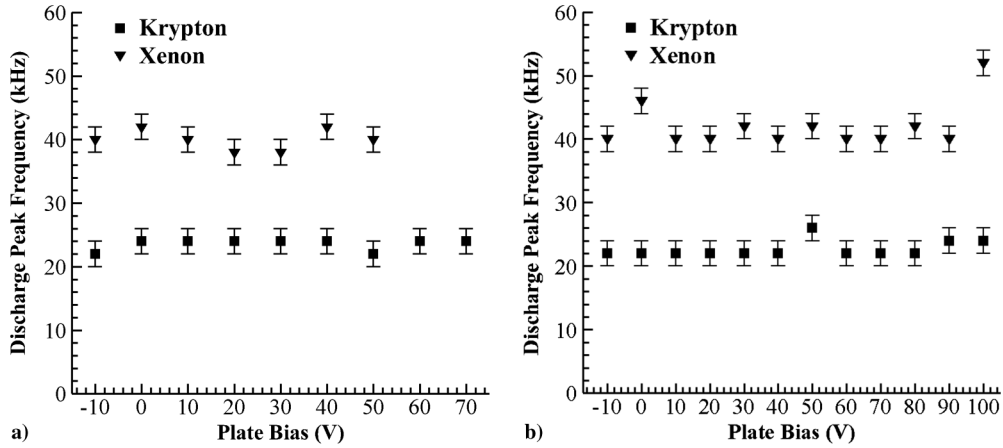


Fig. 12 Peak frequency of the T-40 HET discharge current as a function of a) axial and b) radial plate bias voltages.

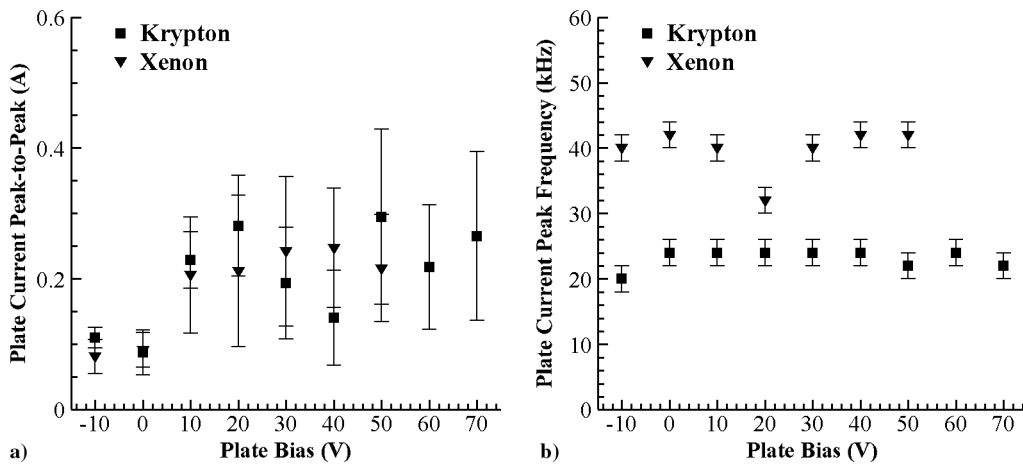


Fig. 13 Average a) peak-to-peak value and b) peak frequency of the current collected by the axial plate as a function of axial plate bias voltage.

operation ( $23 \pm 2$  kHz) and xenon operation ( $40 \pm 3$  kHz) are identical to the corresponding peak frequencies of the discharge current. This suggests that, in a time-resolved sense, current collection by the axial plate is driven by the HET discharge. Taken together, the peak-to-peak values and peak frequencies of the current collected by the axial plate indicate that coupling of the oscillation characteristics between the discharge and test plate currents is invariant with thruster propellant and plate bias. It should be noted that an anomalous drop in axial plate current peak frequency was observed at an axial plate bias of 20 V during xenon operation. Although repeatable, the cause of the decrease is not known. Similar analyses could not be performed for the radial plate current due to the much smaller signal-to-noise ratio associated with these values, thus restricting the analysis of radial plate coupling to the time-averaged characteristics discussed in Sec. III.

To further investigate the coupling of the current collected by the test plates to the T-40 HET discharge current, a statistical correlation analysis was performed to determine the Pearson correlation coefficient  $\rho$  between the two currents for xenon operation. The Pearson correlation coefficient can be calculated as a function of the covariance  $cov(X, Y)$  and standard deviations  $\sigma_X$  and  $\sigma_Y$  of the two waveforms, as shown in Eq. (2) [27]:

$$\rho = \frac{cov(X, Y)}{\sigma_X \sigma_Y} \quad (2)$$

Correlation coefficient magnitudes near unity indicate strong correlation, whereas coefficient values near zero indicate weak correlation [54]. Because the electron current collected by the test plate is recorded as positive current, a positive correlation coefficient

indicates that increases in discharge current are correlated with increased electron current collection on the test plate; similarly, a negative correlation coefficient indicates that increases in discharge current are correlated with increases in ion current collection on the test plate.

The Pearson correlation coefficient between the discharge current and the current collected by the axial plate is plotted as a function of axial plate bias in Fig. 14. As shown in Fig. 14, the average magnitude of the correlation coefficient between the two currents is approximately equal to zero at plate biases of  $-10$  and  $0$  V and approximately equal to

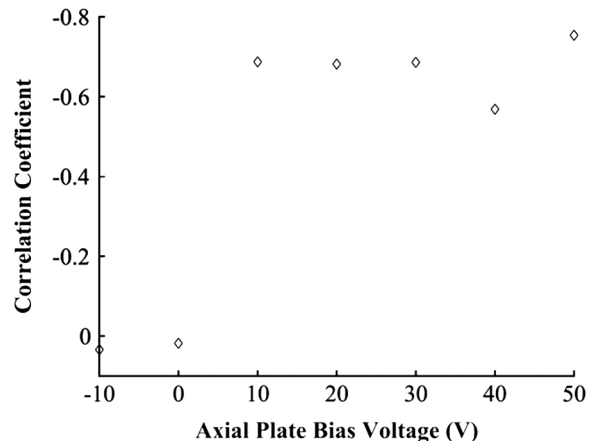


Fig. 14 Pearson correlation coefficient between the T-40 HET discharge current and axial plate current for xenon operation.

–0.7 at plate biases of 10 to 50 V. This observed trend in correlation coefficients as a function of axial plate bias can be explained by the changing current collection properties of the plate as a function of plate bias. For bias voltages between –10 and 0 V, the I–V characteristic of the plate is in the ion saturation region and very little current is collected. Because of the very low magnitude of the collected current, almost no correlation exists between the discharge current and the current collected by the axial plate. For bias voltages above 10 V, the I–V characteristic of the plate is in the electron saturation region and a significant fraction of the discharge current is collected by the axial plate [42,43]. The current collection of the axial plate in the electron saturation region is driven by the local plasma properties near the plate, which have been shown to propagate axially through the thruster plume at a rate equal to the ion transit velocity and at a frequency closely correlated to the peak frequency of the discharge current [52]. Therefore, the strong negative correlation between the discharge current and the current collected by the axial plate at plate biases from 10 to 50 V is expected and is a result of increased axial plate ion collection (and thus a reduced net collected electron current) caused by the downstream propagation of fluctuations from the thruster to the axial plate.

To determine the statistical significance of the correlation coefficients, the  $P$  value of each correlation pair is calculated using a standard null hypothesis test. In this test, it is assumed that the two signals are uncorrelated and a  $P$  value is computed in order to attempt to prove the validity of this initial null hypothesis [55]. A  $P$  value greater than 0.05 indicates that the null hypothesis should be accepted and that the observed correlation is likely the product of random chance, whereas a  $P$  value less than 0.05 indicates that the null hypothesis should be rejected and that the observed correlation is statistically significant [55]. The  $P$  value of each correlation coefficient shown in Fig. 14 is orders of magnitude lower than 0.05, which indicates that the Pearson correlation coefficients are statistically significant and not due to random chance. These trends were largely the same for krypton operation at similar axial plate bias voltages. The computed correlation coefficients suggest that, in a time-resolved sense, current collection by the axial plate is driven by the HET discharge.

### 3. Impact of Facility Pressure on Plate Current Collection

In previous work performed with the 3.4 kW T-140 HET, strong correlation was observed between the discharge current and the current collected by the grounded radial plate. Because the radial plate was located in the wings of the HET plume, the plasma environment near the plate was dominated by CEX ions and electrons; thus, current collection by the plate was driven by the local number density of these species. Because the production of CEX ions has been shown to be driven by the thruster discharge, these ions were attributed as the most likely coupling pathway to the radial plate [28].

Contrary to results found in previous work with the T-140 HET, no correlation was observed between the discharge current and the

current collected by the radial plate during testing of the T-40 HET. The reason for this was likely the difference in facility background pressure between the two tests. The facility pressure during T-140 HET operation was  $7.3 \times 10^{-6}$  torr, which was approximately seven times greater than the corresponding pressure observed during testing of the T-40 HET performed in this work [28]. Previous work with backpressure facility effects has shown that the number of CEX ions in the plume increased with increased facility operating pressure [7,15,18,19,28]. Therefore, far fewer CEX ions were present during operation of the T-40 HET. The dearth of CEX ions prevented the same coupling pathway observed between the grounded radial plate and the T-140 HET discharge current from developing in the T-40 HET test. Because the test facility walls represented an artificial current pathway, the removal of this coupling at lower facility pressures was more representative of the onorbit plume electrical boundary conditions [48]. These results indicated a potential coupling between electrical and pressure facility effects.

## IV. Results and Discussion: Plume Properties

To further examine the link between HET–facility electrical coupling and plume ion current density profile, Faraday probe measurements were taken to examine the effect of test plate bias on plume properties. Figures 15a and 15b show the 95% divergence half-angle of the T-40 HET plume during operation with krypton and xenon as a function of axial and radial plate bias, respectively; and Figs. 16a and 16b show the T-40 HET plume ion beam current during operation of both propellants as a function of axial and radial plate bias, respectively. As shown in Fig. 15, across all axial and radial plate biases, krypton operation resulted in an average divergence half-angle of 33 deg and an ion beam current of 0.57 A; whereas xenon operation produced an average divergence half-angle and average ion beam current of 30 deg and 0.76 A, respectively. The higher divergence half-angle and lower beam current during krypton operation were consistent with the findings of previous studies [34,45]. It is important to note that the beam divergence half-angle varied by less than 6% during krypton operation and less than 5% during xenon operation across all axial and radial plate biases.

There is a similar lack of variation for ion beam current with radial plate bias. As shown in Fig. 16, across all radial plate biases, the measured ion beam current during both krypton and xenon operation varies by less than 4%. A small monotonic increase in ion beam current as a function of axial plate voltage is observed during operation with both propellants; specifically, the ion beam current increases by 11% during krypton operation and 7% during xenon operation as the axial plate bias is changed from –10 to 100 V and –10 to 60 V during krypton and xenon operations, respectively. As discussed in previous work, this trend is likely not a function of varying thruster performance and is instead caused by an increase in current collection in the wings of the HET plume driven by the

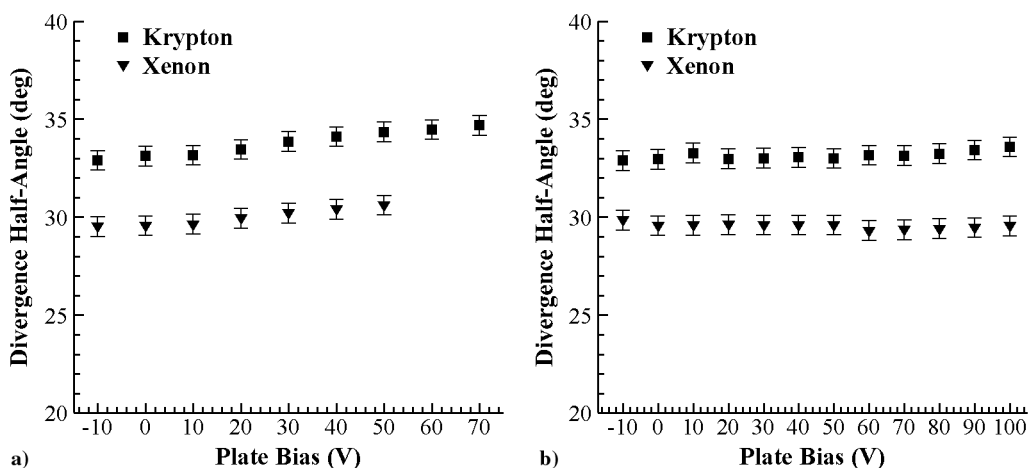


Fig. 15 Plume divergence half-angle of the T-40 HET a function of a) axial and b) radial plate biases.

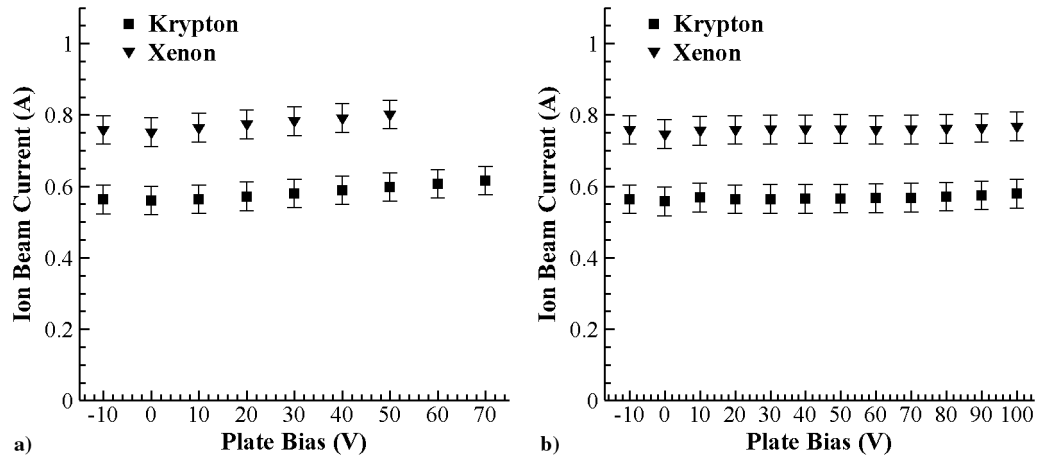


Fig. 16 Plume ion beam current of the T-40 HET as a function of a) axial and b) radial plate biases.

increasing difference between the Faraday probe bias and plume plasma potential at higher axial plate biases [29]. It is important to note that the magnitude of these effects is similar for operation with xenon and krypton and that, when these effects are accounted for, the ion current density profile of the plume appears to be unaffected by plate bias during operation with both krypton and xenon propellants.

## V. Conclusions

This work experimentally characterized the role of the conductive test facility walls in the circuit of the krypton-operated 200 W T-40 HET and compared the findings to data taken during xenon operation to determine the effect of propellant species on facility–HET electrical coupling. Measurements of the ion current profile and the time-resolved characteristics of the discharge and plate currents supported previous findings by showing that thruster oscillation characteristics were unaffected by facility bias. Plate bias was shown to affect the cathode-to-ground voltage during operation with both propellants, and the onset of one-to-one coupling between these parameters occurred at higher voltages for krypton relative to xenon. Current-voltage sweeps of the test plates showed that, when normalized by the discharge current, the percentage of current collected by the axial and radial test plates in the ion and electron saturation regimes collapsed to a common value. This value matched the one for the 3.4 kW T-140 HET. Taken together, these results suggest that the discharge current (due to its relationship to plume ion current density) can be used to scale the coupling between the HET and the facility surfaces in the ion and electron saturation regimes for the employed test facility.

Measurements taken of the current collected by the grounded test plates and of the plate floating voltages indicate that the plume ion current density profile controls the nature of the facility–HET coupling. Specifically, current collection by the axial facility surfaces was shown to be related to the centerline ion current density; the lower ion current density of the krypton-operated HET plume resulted in lower magnitude axial floating plate voltages and the collection of a lower percentage of the discharge current by the grounded axial plate. However, current collection of the radial facility surfaces was strongly impacted by the shape of the ion current density profile. Specifically, the higher plume divergence half-angle associated with krypton operation resulted in the grounded radial plate collecting a net ion current as compared to the net electron current collected during xenon operation. Taken together, these results suggest that both the magnitude and shape of the plume ion current density profile can affect how the facility walls electrically couple to the HET circuit. Because the plume ion current density profile has been shown to be sensitive to a variety of operating parameters including discharge voltage and background pressure, this observation suggests that electrical facility effects for a given HET may not be able to be universally characterized but, rather, must be characterized for each unique operating point and test environment.

## Acknowledgments

Jason Frieman, Nathan Brown, and Connie Liu are supported by the National Science Foundation Graduate Research Fellowship under grant no. DGE-1148903. Jason Frieman is also supported by an Achievement Reward for College Scientists award sponsored by the Lockheed Martin Corporation. The authors would like to thank Sam Langendorf for his very helpful assistance in the collection of data for this paper.

## References

- [1] Brophy, J. R., Friedman, L., and Culick, F., "Asteroid Retrieval Feasibility," *2012 IEEE Aerospace Conference*, IEEE Publ., Piscataway, NJ, 2012, pp. 1–16. doi:10.1109/AERO.2012.6187031
- [2] Herscovitz, J., Zuckerman, Z., and Lev, D., "Electric Propulsion Developments at Rafael," *34th International Electric Propulsion Conference*, Electric Rocket Propulsion Soc., IEPC Paper 2015-030, Fairview Park, OH, 2015.
- [3] Andrenucci, M., Berti, M., Biagioni, L., Cesari, U., Falorni, R., Milanese, L., and Saverdi, M., "The New EP Test Facilities at Centrospazio and Alta," *28th International Electric Propulsion Conference*, Electric Rocket Propulsion Soc., IEPC Paper 2003-229, Fairview Park, OH, 2003.
- [4] Jacobson, D., Manzella, D., Hofer, R., and Peterson, P., "NASA's 2004 Hall Thruster Program," *40th AIAA/ASME/SAE/ASEE Joint Propulsion Conference and Exhibit*, AIAA Paper 2004-3600, 2004. doi:10.2514/6.2004-3600
- [5] Tighe, W. G., Spektor, R., Diamant, K., and Kamhawi, H., "Effects of Background Pressure on the NASA 173M Hall Current Thruster Performance," *34th International Electric Propulsion Conference*, Electric Rocket Propulsion Soc., IEPC Paper 2015-152, Fairview Park, OH, 2015.
- [6] Reid, B. M., "Empirically-Derived Corrections for Facility Effects in Performance and Plume Measurements of Hall Thrusters," *34th International Electric Propulsion Conference*, Electric Rocket Propulsion Soc., IEPC Paper 2015-362, Fairview Park, OH, 2015.
- [7] Brown, D. L., and Gallimore, A. D., "Evaluation of Plume Divergence and Facility Effects on Far-Field Faraday Probe Current Density Profiles," *31st International Electric Propulsion Conference*, Electric Rocket Propulsion Soc., IEPC Paper 2009-030, Fairview Park, OH, 2009.
- [8] Diamant, K. D., Liang, R., and Corey, R. L., "The Effect of Background Pressure on SPT-100 Hall Thruster Performance," *50th AIAA/ASME/SAE/ASEE Joint Propulsion Conference*, AIAA Paper 2014-3710, 2014. doi:10.2514/6.2014-3710
- [9] Goebel, D. M., and Katz, I., *Fundamentals of Electric Propulsion: Ion and Hall Thrusters*, Wiley, Hoboken, NJ, 2008, pp. 325–384, 463–467.
- [10] Hofer, R. R., Peterson, P. Y., and Gallimore, A. D., "Characterizing Vacuum Facility Backpressure Effects on the Performance of a Hall Thruster," *27th International Electric Propulsion Conference*, Electric Rocket Propulsion Soc., IEPC Paper 2001-045, Fairview Park, OH, 2001.
- [11] Hofer, R. R., and Anderson, J. R., "Finite Pressure Effects in Magnetically Shielded Hall Thrusters," *50th AIAA/ASME/SAE/ASEE Joint Propulsion Conference*, AIAA Paper 2014-3709, 2014. doi:10.2514/6.2014-3709

- [12] Huang, W., Kamhawi, H., Lobbia, R. B., and Brown, D. L., "Effect of Background Pressure on the Plasma Oscillation Characteristics of the HiVHAc Hall Thruster," *50th AIAA/ASME/SAE/ASEE Joint Propulsion Conference*, AIAA Paper 2014-3708, 2014.  
doi:10.2514/6.2014-3708
- [13] Kamhawi, H., Huang, W., Haag, T., and Spektor, R., "Investigation of the Effects of Facility Background Pressure on the Performance and Operation of the High Voltage Hall Accelerator," *50th AIAA/ASME/SAE/ASEE Joint Propulsion Conference*, AIAA Paper 2014-3707, 2014.  
doi:10.2514/6.2014-3707
- [14] Nakles, M. R., and Hargus, W. A., "Background Pressure Effects on Ion Velocity Distribution within a Medium-Power Hall Thruster," *Journal of Propulsion and Power*, Vol. 27, No. 4, 2011, pp. 737–743.  
doi:10.2514/1.48027
- [15] Walker, M. L. R., Victor, A. L., Hofer, R. R., and Gallimore, A. D., "Effect of Backpressure on Ion Current Density Measurements in Hall Thruster Plumes," *Journal of Propulsion and Power*, Vol. 21, No. 3, 2005, pp. 408–415.  
doi:10.2514/1.7713
- [16] Randolph, T., Kim, V., Kaufman, H. R., Kozubsky, K., Zhurin, V. V., and Day, M., "Facility Effects on Stationary Plasma Thruster Testing," *23rd International Electric Propulsion Conference*, Electric Rocket Propulsion Soc., IEPC Paper 1993-093, Fairview Park, OH, 1993.
- [17] Reid, B. M., "The Influence of Neutral Flow Rate in the Operation of Hall Thrusters," Ph.D. Dissertation, Aerospace Engineering Dept., Univ. of Michigan, Ann Arbor, MI, 2009, pp. 306–319.
- [18] Walker, M. L. R., "Effects of Facility Backpressure on the Performance and Plume of a Hall Thruster," Ph.D. Dissertation, Aerospace Engineering Dept., Univ. of Michigan, Ann Arbor, MI, 2005, pp. 126–135.
- [19] Walker, M., Hofer, R., and Gallimore, A., "The Effects of Nude Faraday Probe Design and Vacuum Facility Backpressure on the Measured Ion Current Density Profile of Hall Thruster Plumes," *38th AIAA/ASME/SAE/ASEE Joint Propulsion Conference and Exhibit*, AIAA Paper 2002-4253, 2002.  
doi:10.2514/6.2002-4253
- [20] Kamhawi, H., Haag, T., Huang, W., Yim, J., Herman, D. A., Peterson, P. Y., Williams, G., Gilland, J., Hofer, R. R., and Mikellides, I. G., "Performance, Facility Pressure Effects, and Stability Characterization Tests of NASA's 12.5-kW Hall Effect Rocket with Magnetic Shielding Thruster," *52nd AIAA/SAE/ASEE Joint Propulsion Conference*, AIAA Paper 2016-4826, 2016.  
doi:10.2514/6.2016-4826
- [21] Kamhawi, H., Huang, W., Haag, T., Shastry, R., Thomas, R., Yim, J., Herman, D., Williams, G., Myers, J., and Hofer, R. R., "Performance and Facility Background Pressure Characterization Tests of NASA's 12.5-kW Hall Effect Rocket with Magnetic Shielding Thruster," *34th International Electric Propulsion Conference*, Electric Rocket Propulsion Soc., IEPC Paper 2015-07, Fairview Park, OH, 2015.
- [22] Huang, W., Kamhawi, H., and Haag, T., "Facility Effect Characterization Test of NASA's HERMeS Hall Thruster," *52nd AIAA/SAE/ASEE Joint Propulsion Conference*, AIAA Paper 2016-4828, 2016.  
doi:10.2514/6.2016-4828
- [23] Peterson, P. Y., Kamhawi, H., Huang, W., Williams, G., Gilland, J. H., Yim, J., Hofer, R. R., and Herman, D. A., "NASA's HERMeS Hall Thruster Electrical Configuration Characterization," *52nd AIAA/SAE/ASEE Joint Propulsion Conference*, AIAA Paper 2016-5027, 2016.  
doi:10.2514/6.2016-5027
- [24] Byers, D., and Dankanich, J., "A Review of Facility Effects on Hall Effect Thrusters," *31st International Electric Propulsion Conference*, Electric Rocket Propulsion Soc., IEPC Paper 2009-067, Fairview Park, OH, 2009.
- [25] Walker, M. L. R., and Gallimore, A. D., "Neutral Density Map of Hall Thruster Plume Expansion in a Vacuum Chamber," *Review of Scientific Instruments*, Vol. 76, No. 5, 2005, Paper 053509.  
doi:10.1063/1.1915011
- [26] Frieman, J. D., Walker, J. A., Walker, M. L. R., Khayms, V., and King, D. Q., "Electrical Facility Effects on Hall Thruster Cathode Coupling: Performance and Plume Properties," *Journal of Propulsion and Power*, Vol. 32, No. 1, 2016, pp. 251–264.  
doi:10.2514/1.B35683
- [27] Frieman, J. D., King, S. T., Walker, M. L. R., Khayms, V., and King, D., "Role of a Conducting Vacuum Chamber in the Hall Effect Thruster Electrical Circuit," *Journal of Propulsion and Power*, Vol. 30, No. 6, 2014, pp. 1471–1479.  
doi:10.2514/1.B35308
- [28] Walker, J. A., Frieman, J. D., Walker, M. L. R., Khayms, V., King, D., and Peterson, P. Y., "Electrical Facility Effects on Hall-Effect-Thruster Cathode Coupling: Discharge Oscillations and Facility Coupling," *Journal of Propulsion and Power*, Vol. 32, No. 4, 2016, pp. 844–855.  
doi:10.2514/1.B35835
- [29] Frieman, J. D., Brown, N. P., Liu, C. Y., Liu, T. M., Walker, M. L. R., Khayms, V., and King, D. Q., "Electrical Facility Effects on Faraday Probe Measurement," *Journal of Propulsion and Power*, advance online publication, 4 Aug. 2017.
- [30] Kieckhafer, A., and King, L. B., "Energetics of Propellant Options for High-Power Hall Thrusters," *Journal of Propulsion and Power*, Vol. 23, No. 1, 2007, pp. 21–26.  
doi:10.2514/1.16376
- [31] Vincenti, W. G., and Kruger, C. H., *Introduction to Physical Gas Dynamics*, Krieger, Malabar, FL, 2002, pp. 12–15.
- [32] Hargus, W. A., Jr., Tango, L. J., and Nakles, M. R., "Background Pressure Effects on Krypton Hall Effect Thruster Internal Acceleration," *33rd International Electric Propulsion Conference*, Electric Rocket Propulsion Soc., IEPC Paper 2013-340, Washington, D.C., 2013.
- [33] Kieckhafer, A. W., and Walker, M. L. R., "Recirculating Liquid Nitrogen System for Operation of Cryogenic Pumps," *32nd International Electric Propulsion Conference*, Electric Rocket Propulsion Soc., IEPC Paper 2011-217, Fairview Park, OH, 2011.
- [34] Frieman, J. D., Liu, T., Walker, M. L., Makela, J., Mathers, A., and Peterson, P. Y., "Performance Evaluation of the T-40 Low-Power Hall Current Thruster," *52nd AIAA/SAE/ASEE Joint Propulsion Conference*, AIAA Paper 2016-4833, 2016.  
doi:10.2514/6.2016-4833
- [35] Dushman, S., and Lafferty, J. M., *Scientific Foundations of Vacuum Technique*, Wiley, New York, 1962, pp. 349–359.
- [36] Snyder, J. S., Baldwin, J., Frieman, J. D., Walker, M. L. R., Hicks, N. S., Polzin, K. A., and Singleton, J. T., "Recommended Practice for Flow Control and Measurement in Electric Propulsion Testing," *Journal of Propulsion and Power*, Vol. 33, No. 3, 2017, pp. 556–565.  
doi:10.2514/1.B35644
- [37] Washeleski, R., and King, L., "Characterization of the Plasma Plume from a LaB6 Cathode: A Comparison of Probe Techniques," *45th AIAA/ASME/SAE/ASEE Joint Propulsion Conference and Exhibit*, AIAA Paper 2009-5199, 2009.  
doi:10.2514/6.2009-5199
- [38] Sommerville, J. D., and King, L. B., "Hall-Effect Thruster–Cathode Coupling, Part I: Efficiency Improvements from an Extended Outer Pole," *Journal of Propulsion and Power*, Vol. 27, No. 4, 2011, pp. 744–753.  
doi:10.2514/1.50123
- [39] Sommerville, J. D., and King, L. B., "Hall-Effect Thruster–Cathode Coupling, Part II: Ion Beam and Near-Field Plume," *Journal of Propulsion and Power*, Vol. 27, No. 4, 2011, pp. 754–767.  
doi:10.2514/1.50124
- [40] Litvak, A., Raitses, Y., and Fisch, N., "Experimental Studies of High-Frequency Oscillations in Hall Thrusters," *38th AIAA/ASME/SAE/ASEE Joint Propulsion Conference and Exhibit*, AIAA Paper 2002-3825, 2002.  
doi:10.2514/6.2002-3825
- [41] Kurzyrna, J., Mazouffre, S., Lazurenko, A., Albarède, L., Bonhomme, G., Makowski, K., Dudeck, M., and Peradzyński, Z., "Spectral Analysis of Hall-Effect Thruster Plasma Oscillations Based on the Empirical Mode Decomposition," *Physics of Plasmas*, Vol. 12, No. 12, 2005, Paper 123506.  
doi:10.1063/1.2145020
- [42] Demidov, V. I., Ratynskaia, S. V., and Rypdal, K., "Electric Probes for Plasmas: The Link Between Theory and Instrument," *Review of Scientific Instruments*, Vol. 73, No. 10, 2002, pp. 3409–3439.  
doi:10.1063/1.1505099
- [43] Piel, A., *Plasma Physics: An Introduction to Laboratory, Space, and Fusion Plasmas*, Springer-Verlag, Berlin, 2010, pp. 1441–1426.
- [44] Xu, K. G., "Ion Collimation and In-Channel Potential Shaping Using In-Channel Electrodes for Hall Effect Thrusters," Ph.D. Dissertation, Aerospace Engineering Dept., Georgia Inst. of Technology, Atlanta, GA, 2012, pp. 48–53.
- [45] Linnell, J. A., "An Evaluation of Krypton Propellant in Hall Thrusters," Ph.D. Dissertation, Aerospace Engineering Dept., Univ. of Michigan, Ann Arbor, MI, 2007, pp. 80–116.
- [46] Peterson, P., Jacobson, D., Manzella, D., and John, J., "The Performance and Wear Characterization of a High-Power High-Isp NASA Hall Thruster," *41st AIAA/ASME/SAE/ASEE Joint Propulsion Conference and Exhibit*, AIAA Paper 2005-4243, 2005.  
doi:10.2514/6.2005-4243
- [47] Jacobson, D., and Manzella, D., "50 kW Class Krypton Hall Thruster Performance," *39th AIAA/ASME/SAE/ASEE Joint Propulsion Conference*

- and Exhibit, AIAA Paper 2003-4550, 2003.  
doi:10.2514/6.2003-4550
- [48] Walker, J. A., Langendorf, S. J., Walker, M. L. R., Khayms, V., King, D., and Pertson, P., "Electrical Facility Effects on Hall Current Thrusters: Electron Termination Pathway Manipulation," *Journal of Propulsion and Power*, Vol. 32, No. 6, 2016, pp. 1365–1377.  
doi:10.2514/1.B35904
- [49] Hofer, R. R., and Gallimore, A. D., "High-Specific Impulse Hall Thrusters, Part 2: Efficiency Analysis," *Journal of Propulsion and Power*, Vol. 22, No. 4, 2006, pp. 732–740.  
doi:10.2514/1.15954
- [50] Linnell, J. A., and Gallimore, A. D., "Efficiency Analysis of a Hall Thruster Operating with Krypton and Xenon," *Journal of Propulsion and Power*, Vol. 22, No. 6, 2006, pp. 1402–1418.  
doi:10.2514/1.19613
- [51] Manzella, D., and Sankovic, J., "Hall Thruster Ion Beam Characterization," *31st Joint Propulsion Conference and Exhibit*, AIAA Paper 1995-2927, 1995.  
doi:10.2514/6.1995-2927
- [52] Jahn, R. G., *Physics of Electric Propulsion*, McGraw-Hill, New York, 1968, pp. 45–67.
- [53] Shin, H., Zhu, W., Xu, L., Donnelly, V. M., and Economou, D. J., "Control of Ion Energy Distributions Using a Pulsed Plasma with Synchronous Bias on a Boundary Electrode," *Plasma Sources Science and Technology*, Vol. 20, No. 5, 2011, Paper 055001.  
doi:10.1088/0963-0252/20/5/055001
- [54] McDonald, M. S., and Gallimore, A. D., "Cathode Position and Orientation Effects on Cathode Coupling in a 6-kW Hall Thruster," *31st International Electric Propulsion Conference*, Electric Rocket Propulsion Soc., IEPC Paper 2009-113, Fairview Park, OH, 2009.
- [55] Sekerak, M. J., "Plasma Oscillations and Operational Modes in Hall Effect Thrusters," Ph.D. Dissertation, Aerospace Engineering Dept., Univ. of Michigan, Ann Arbor, MI, 2014, pp. 55–58.
- [56] Sekerak, M. J., Gallimore, A. D., Brown, D. L., Hofer, R. R., and Polk, J. E., "Mode Transitions in Hall-Effect Thrusters Induced by Variable Magnetic Field Strength," *Journal of Propulsion and Power*, Vol. 32, No. 4, 2016, pp. 903–917.  
doi:10.2514/1.B35709
- [57] Choueiri, E. Y., "Plasma Oscillations in Hall Thrusters," *Physics of Plasmas*, Vol. 8, No. 4, 2001, pp. 1411–1426.  
doi:10.1063/1.1354644
- [58] Zill, D. G., and Wright, W. S., *Advanced Engineering Mathematics*, Jones and Bartlett Learning, Burlington, MA, 2014, pp. 744–773.
- [59] Liu, D., Huffman, R. E., Branam, R. D., and Hargus, W. A., "Ultrahigh-Speed Imaging of Hall-Thruster Discharge Oscillations with Krypton Propellant," *IEEE Transactions on Plasma Science*, Vol. 39, No. 11, 2011, pp. 2926–2927.  
doi:10.1109/TPS.2011.2146282
- [60] Lobbia, R. B., Sekerak, M. J., Liang, R., and Gallimore, A. D., "High-Speed Dual Langmuir Probe Measurements of the Plasma Properties and EEDFs in a HET Plume," *32nd International Electric Propulsion Conference*, Electric Rocket Propulsion Soc., IEPC Paper 2011-168, Fairview Park, OH, 2011.
- [61] Lin, L., Hedayat, A. S., and Wu, W., *Statistical Tools for Measuring Agreement*, Springer-Verlag, New York, 2012, pp. 13–0.  
doi:10.1007/978-1-4614-0562-7

J. Blandino  
Associate Editor